Ultrasonics 83 (2018) 94–102

Contents lists available at ScienceDirect

Ultrasonics

journal homepage: www.elsevier.com/locate/ultras

The role of ultrasonic cavitation in refining the microstructure of aluminum based nanocomposites during the solidification process

Yang Xuan, Laurentiu Nastac *

The University of Alabama, Department of Metallurgical and Materials Engineering, Box 870202, Tuscaloosa, AL 35487, USA

ARTICLE INFO

Article history:
Received 20 February 2017
Received in revised form 23 June 2017
Accepted 30 June 2017
Available online 1 July 2017

Keywords:
Ultrasonic cavitation processing
Solidification processing
A356-matrix-nanocomposites
Al_2O_3 nanoparticles
Microstructure
Grain refinement
Eutectic modification

ABSTRACT

Recent studies showed that the microstructure and mechanical properties of aluminum based nanocomposites can be significantly improved when ultrasonic cavitation and solidification processing is used. This is because ultrasonic cavitation processing plays an important role not only in degassing and dispersion of the nanoparticles, but also in breaking up the dendritic grains and refining the as-cast microstructure.

In the present study, A356 alloy and Al_2O_3 nanoparticles are used as the matrix alloy and the reinforcement, respectively. Nanoparticles were added into the molten A356 alloy and dispersed via ultrasonic cavitation processing. Ultrasonic cavitation was applied over various temperature ranges during molten alloy cooling and solidification to investigate the grain structure formation and the nanoparticle dispersion behavior. Optical Microscopy and Scanning Electron Microscopy were used to investigate in detail the differences in the microstructure characteristics and the nanoparticle distribution. Experimental results indicated that the ultrasonic cavitation processing and Al_2O_3 nanoparticles play an important role for microstructure refinement. In addition, it was shown in this study that the Al_2O_3 nanoparticles modified the eutectic phase.

1. Introduction

As a result of the high specific strength, high wear resistance, controllable expansion coefficient and economic efficiency, aluminum metal matrix composites (MMCs) have been treated as suitable materials in automobile, aerospace and military applications [1–8]. However, the micro-size ceramic particles, which were used as reinforcement in MMCs, could significantly decrease the ductility of these composite materials. It has been recently proven that using nano-size ceramic particles as reinforcement to fabricate metal-matrix-nano-composites (MMNCs) can distinctly improve the matrix properties, while maintaining good ductility and high temperature creep resistance [9–13]. The fabrication of high-quality MMNCs depends on the uniform dispersion of the nano-size ceramic particles into the matrix.

Mechanical stirring is widely used to produce MMCs. However, it is extremely challenging to fabricate MMNCs via the traditional mechanical stirring method. Because of the high specific surface area of nanoparticles, it is difficult for mechanical stirring to distribute and disperse nanoparticles uniformly into the molten alloy. Moreover, the poor wettability between the molten alloys and the ceramic nanoparticles would cause nanoparticles to re-agglomerate and float on the liquid surface after mechanical stirring stops [14].

Ultrasonic stirring technology (UST) has been proved highly effective to fabricate MMNCs by many research studies [1–11].

Ultrasonic stirring generates nonlinear effects such as acoustic streaming and cavitation into the liquid [18]. Streaming could increase the transfer of small particles in the melt, equalize the melt solute concentration and temperature, and break the dendrites. When ultrasonic cavitation occurs in the melt, the pulsating cavitation bubbles would cause fluctuations of the melt temperature and pressure. Transient and extremely high temperatures (possibly >5000 K) could significantly enhance the wettability between the nanoparticles and the metal melts. The implosive impact generated by local transient high pressures (>1000 atm.) is strong enough to break up the clustered nanoparticles. In addition, the strong streaming generated by ultrasonic stirring can help disperse the nanoparticles uniformly into the liquid. Research studies have shown that by introducing UST into the metal melt for 15–60 min, the nanoparticle clusters could be successfully broken and dispersed very well into the molten metal [9,10,15–17].

During the alloy solidification process, UST can also be used to refine the metallic alloy microstructure. Two hypotheses have been

* Corresponding author.
E-mail address: lnastac@eng.ua.edu (L. Nastac).

http://dx.doi.org/10.1016/j.ultras.2017.06.023
0041-624X/

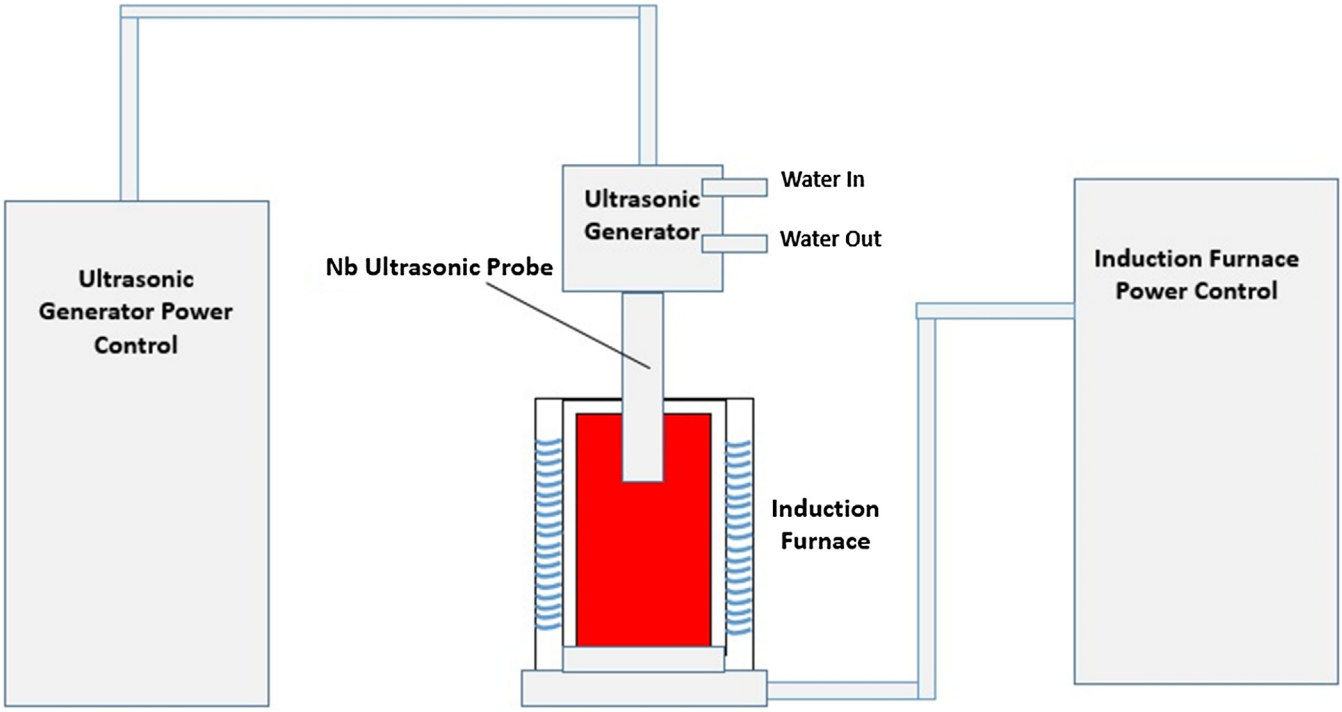

Fig. 1. Sketch of the ultrasonic cavitation processing system.

proposed to explain the effect of the ultrasonic cavitation refinement during solidification [10,19–22]. The first hypothesis is that the ultrasound will increase the nucleation potential of the melt. When applying ultrasonic cavitation, the temperature and pressure characteristics of the melt will change periodically at high frequencies, which can then increase the number of local nuclei. In addition, strong convection produced by ultrasonic cavitation can promote the diffusion of solute to increase the number of nuclei in the melt. The second hypothesis is that the ultrasonic cavitation can produce shock waves, resulting in the breakage of the dendrite tips, which contributes to the refinement of the microstructure.

There are several factors that could influence the rate of microstructure refinement by applying UST during solidification. Ramirez et al. [23] indicated that the ultrasonic grain refinement exhibited strong dependence on the solute content by comparing the microstructure of pure Mg, binary Mg-Al alloys, and commercial Mg-based alloys, which were fabricated by applying UST during solidification. Qian et al. [24] proposed that the grain size of Mg- Al alloys increased with the increasing distance from the radiator, which could be explained by the fade of the UST convection/intensity along the distance from the radiator. It was also proved that the grain size distribution is symmetrical along the probe, which means that the grain size distribution overlaps at the same distance from the radiator.

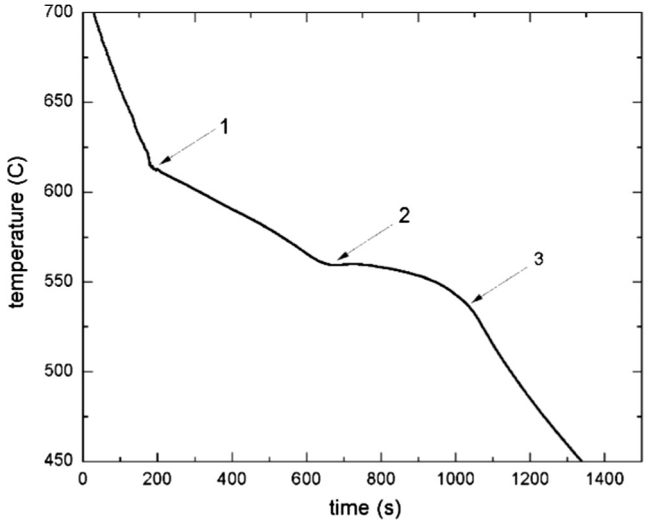

Fig. 2. Temperature – time curve of the processed A356 alloy.

Another important factor that could affect the microstructure refinement is the UST processing temperature. Experimental results suggest that the application of UST in the molten alloys has no significant effect on the primary phase morphology, but would help to modify the secondary phases and eutectic phase [25–29]. Jung et al. [27] applied UST over the temperature range of 750–700 °C, which is higher than the solidus temperature of the processed alloy, on near-eutectic commercial Al-Si piston alloys. Their results indicated that the UST can greatly decrease the size of the eutectic cells and secondary phases, due to the enhanced and prolonged nucleation of each phase.

A significant number of research studies have identified UST as a promising way to fabricate MMNCs. Recent work [10] has shown that for Al-based nanocomposites, when applying UST during solidification, the added nanoparticles are not the main cause for microstructure refinement, but could help to modify the microstructure. Nevertheless, the temperature effects on the microstructure refinement of MMNCs with UST during solidification have to be studied.

The present study proposed a novel method of fabricating Al-based nanocomposites. The nanocomposites have been fabricated via ultrasonic cavitation using A356 alloy and Al_2O_3 as the matrix and the reinforcement, respectively. The effects of various melting and solidification conditions and of the nanoparticle distribution on both the matrix microstructure and the precipitated secondary phases have been carefully evaluated.

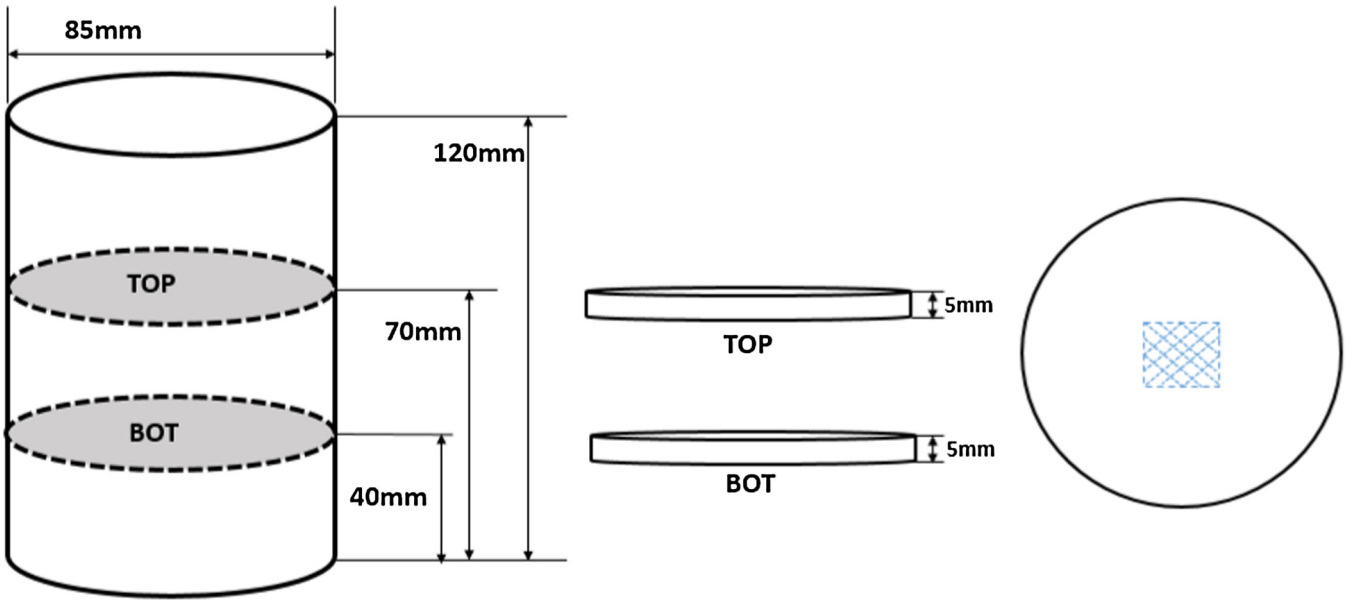

Fig. 3. Schematic of the sectioned cast ingot samples.

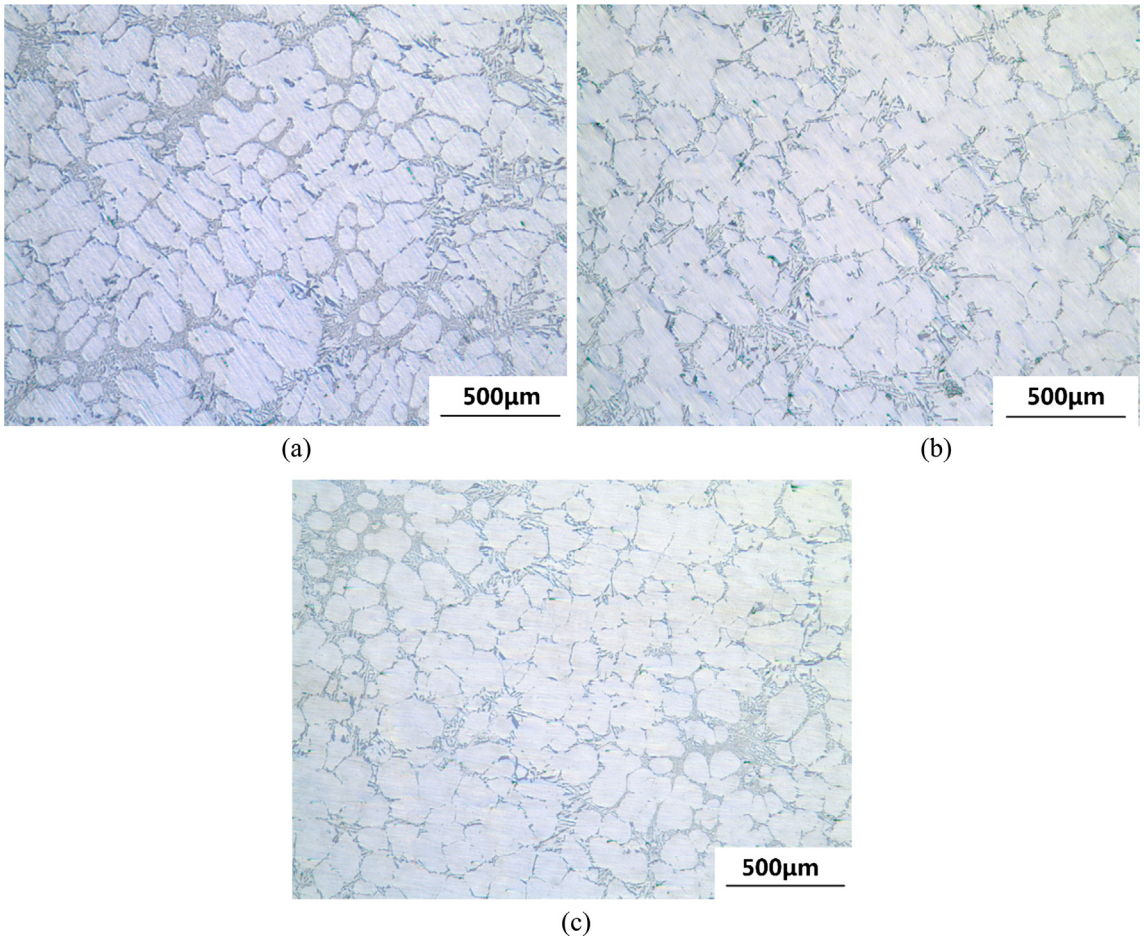

Fig. 4. Optical micrographs of the cast top disks at 50× (a) without UST (b) applied UST over a range of temperatures from 650 °C to 620 °C (c) applied UST over a range of temperatures from 614 °C to 600 °C during solidification.

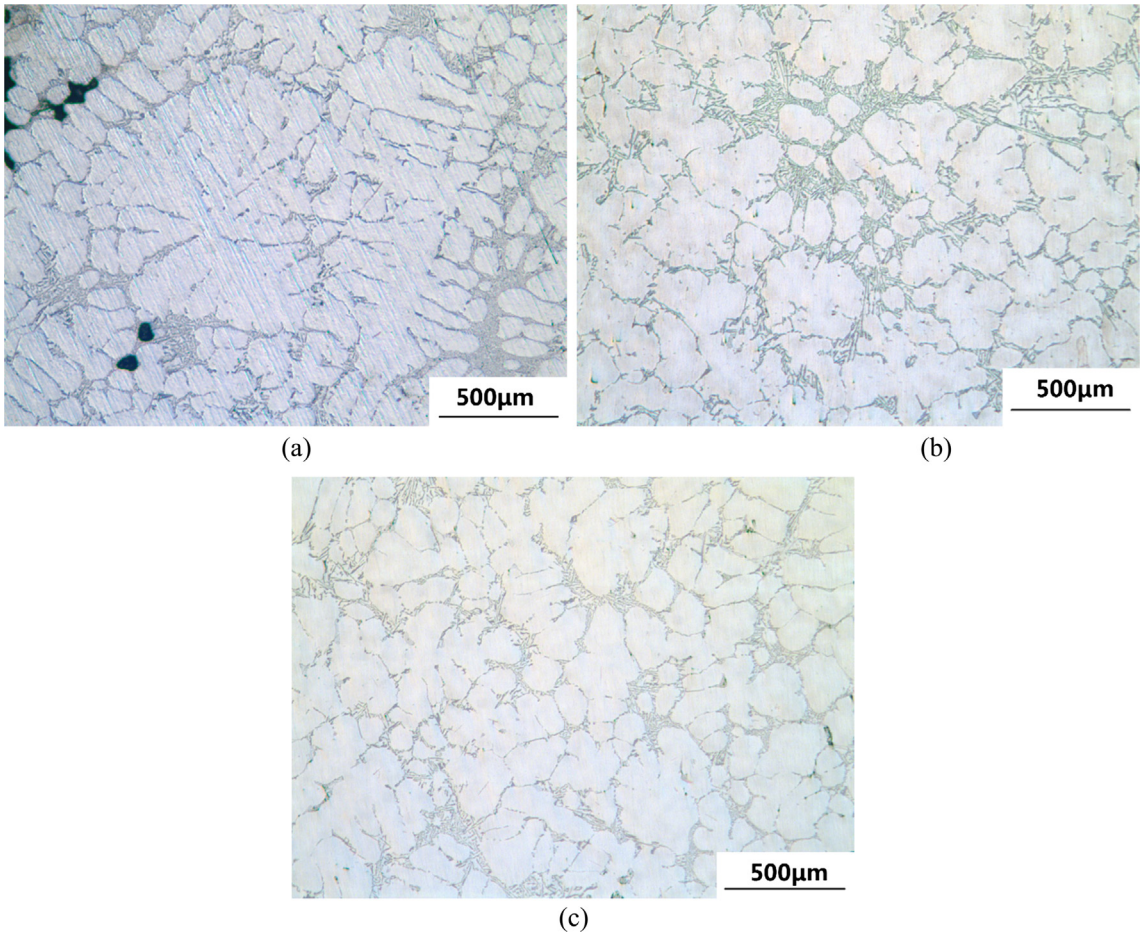

Fig. 5. Optical micrographs of the cast bottom disks at 50× (a) without UST (b) applied UST over a range of temperatures from 650 °C to 620 °C (c) applied UST over a range of temperatures from 614 °C to 600 °C during solidification.

2. Experimental approach

In the present work, commercial aluminum alloy A356 was used as the metallic alloy matrix. Jia et al. [9] indicated that one of the optimum type of nano-size particles is Al_2O_3, and the optimum amount of Al_2O_3 is 1.0 wt.%. Thus, in this study, Al_2O_3 nanoparticles (spherical shape, average diameter of about 20 nm) were used as the reinforcement. The ultrasonic equipment parameters are as follows: maximum power is 2.4 kW; frequency is18 kHz, the diameter of the Nb ultrasonic probe is 40 mm and the probe amplitude is 20 μm. The sketch of the UST system is shown in Fig. 1.

An Inductotherm induction furnace was used to melt the alloy. When the melt temperature reached about 750 °C, the ultrasonic probe was inserted to about 50 mm beneath the melt surface to perform ultrasound cavitation and stirring. 1.0 wt.% Al_2O_3 was added into the cavitation area during a 15 min time-frame. K-type thermocouples inserted 50 mm beneath the melt surface were used to record the temperature–time evolution during the experiment.

In order to minimize the effect of the ultrasonic probe-cooling effect onto the melt, the ultrasonic probe was preheated without turning on the power by inserting it into the melt at about 750 °C. Ultrasonic cavitation processing was controlled by turning on/off the ultrasonic generator power. The temperature–time curve of the melt has been plotted to identify the phase transformation temperature, as shown in Fig. 2. The liquidus temperature of this alloy is about 614 °C (inflexion 1). Inflexion 2 indicates the start of the eutectic phase at about 560 °C. Inflexion 3 shows the end of solidification, which is about 538 °C. Fig. 2 indicated that it takes about 450 s for the melt temperature to drop from 614 °C to 560 °C and about 400 s for the melt temperature to drop from 560 °C to 538 °C.

Based on the temperature–time curve shown in Fig. 2, three types of experiments were designed: (1) without UST processing, (2) above-liquidus UST processing and (3) below-liquidus UST processing. In the process without the use of UST treatment, after 15 min of ultrasonic cavitation processing at 750 °C, the induction furnace power was shut down to let the melt cooled inside the furnace. For the second type of experiment, which is above-liquidus UST processing, the ultrasonic cavitation was applied into the molten alloy over 650–620 °C temperature range and the melt was cooled inside the furnace. The third type of experiment, which is below-liquidus UST processing, was similar with second one but the ultrasonic cavitation processing temperature range was changed to 614–600 °C.

The cast ingots were cylindrical in shape, the ingot diameter is 85 mm and its height is 120 mm. Two small disks were cut from the ingot, as shown in Fig. 3, and labeled as top and bottom, respectively. The disk height is 5mm and the distances from the bottom to the top and the bottom disk were 70 mm and 40 mm, respectively. During UST processing, the ultrasonic probe was inserted to about 50 mm beneath the melt, thus the top disk was the section located below the probe, and the bottom disk was the section located at 30mm below the probe.

Regarding the microstructure analysis, the samples from the disk centers (as shown in Fig. 3) have been prepared by grinding

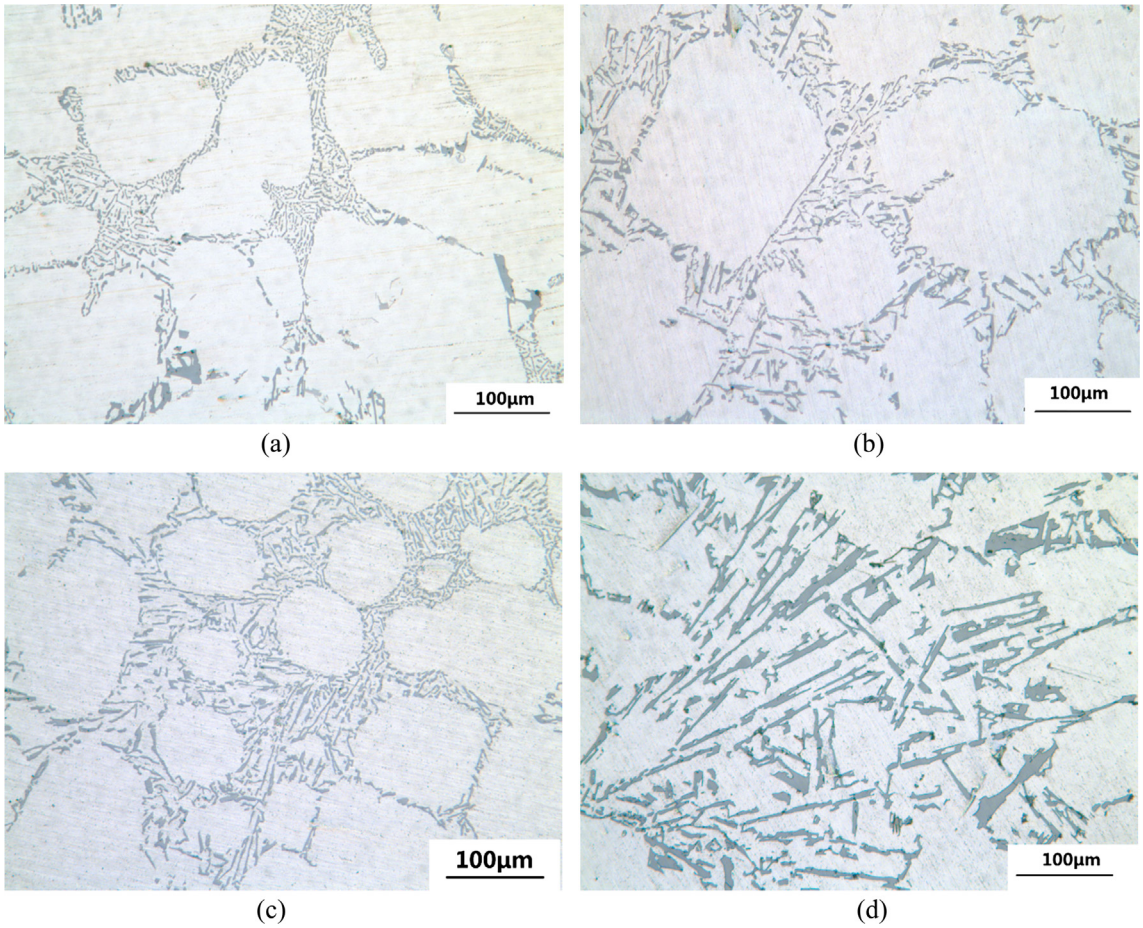

Fig. 6. Eutectic Si phase refinement at 200× (a) without UST (b) applied UST over a range of temperature from 650 °C to 620 °C (c) applied UST over a range of temperature from 614 °C to 600 °C during solidification (d) coarse eutectic Si in all the casting ingots (lamellar morphology, longer than 100 µm).

with 240, 600, 800, 1200 sand papers followed by polishing with 9 µm, 3 µm, and 1 µm water based diamond suspensions. Flick etchant has been used in this study with the following composition: 10 vol.% hydrogen fluoride, 15 vol.% hydrogen chloride and distilled water. All samples have been etched for about 10–15 s. Optical Microscopy (Nikon EPIPHOT 200) and Scanning Electron Microscopy (JEOL 7000) have been used for microstructure characterization and analysis of all samples.

3. Experimental results and discussion

3.1. The microstructure of the top disks

Fig. 4 shows the obtained microstructures of the top disks under three different experimental conditions: (1) without the use of ultrasonic cavitation processing (2) with ultrasonic cavitation processing from 650 °C to 620 °C (which is 6 °C above the liquidus temperature) and (3) with ultrasonic cavitation processing from 614 °C to 600 °C during solidification. Fig. 4(a) indicated that without the application of the ultrasonic cavitation processing during solidification, the microstructure was dendritic in shape with a large dendritic grain size. However, by applying the ultrasonic cavitation during solidification, regardless of the temperature range, the microstructure was refined significantly by changing the grain morphology from dendritic to globular, as shown in Fig. 4 (b) and (c). From the microstructure differences shown in Fig. 4, it can be concluded that for A356 with 1.0 wt.% Al_2O_3 nanoparticles, the ultrasonic cavitation processing plays a key role to refine the alloy microstructure during solidification.

X. Jian et al. [19] indicated that for the A356 alloy, the microstructure refinement can be observed only when the ultrasonic cavitation is applied until the temperature is lower than the liquidus temperature (614 °C) during solidification. In addition, it has been shown that for Al-based alloys without nanoparticles, there is no grain refinement when the ultrasonic cavitation was applied for temperature ranges above the alloy liquidus temperature. However, in the present study, the application of the ultrasonic cavitation from 650 °C to 620 °C (which is 6 °C above the liquidus temperature) still refined the microstructure significantly, as shown in Fig. 4(b). This means that the Al_2O_3 nanoparticles significantly contributed to the refinement of the microstructure during the solidification process. This fact can be explained as follows: the ultrasonic cavitation increases the uniformity of Al_2O_3 nanoparticle dispersion in the liquid and activate these nanoparticles by enhancing the wettability between the molten metal and the nanoparticles, which in turn will increase the nucleation potential of the melt, and consequently change the microstructure from a coarse dendritic to a fine globular morphology [30].

Ultrasonic cavitation refinement during solidification can be explained by the increase in the nucleation potential of the melt and by promoting the fragmentation of the dendrites. In Fig. 4(b), the grain morphology is more like petal-shape and the grain size is larger than that in Fig. 4(c), which indicated that the degree of refinement with ultrasonic cavitation processing from 614 °C to 600 °C during solidification is higher than that with ultrasonic

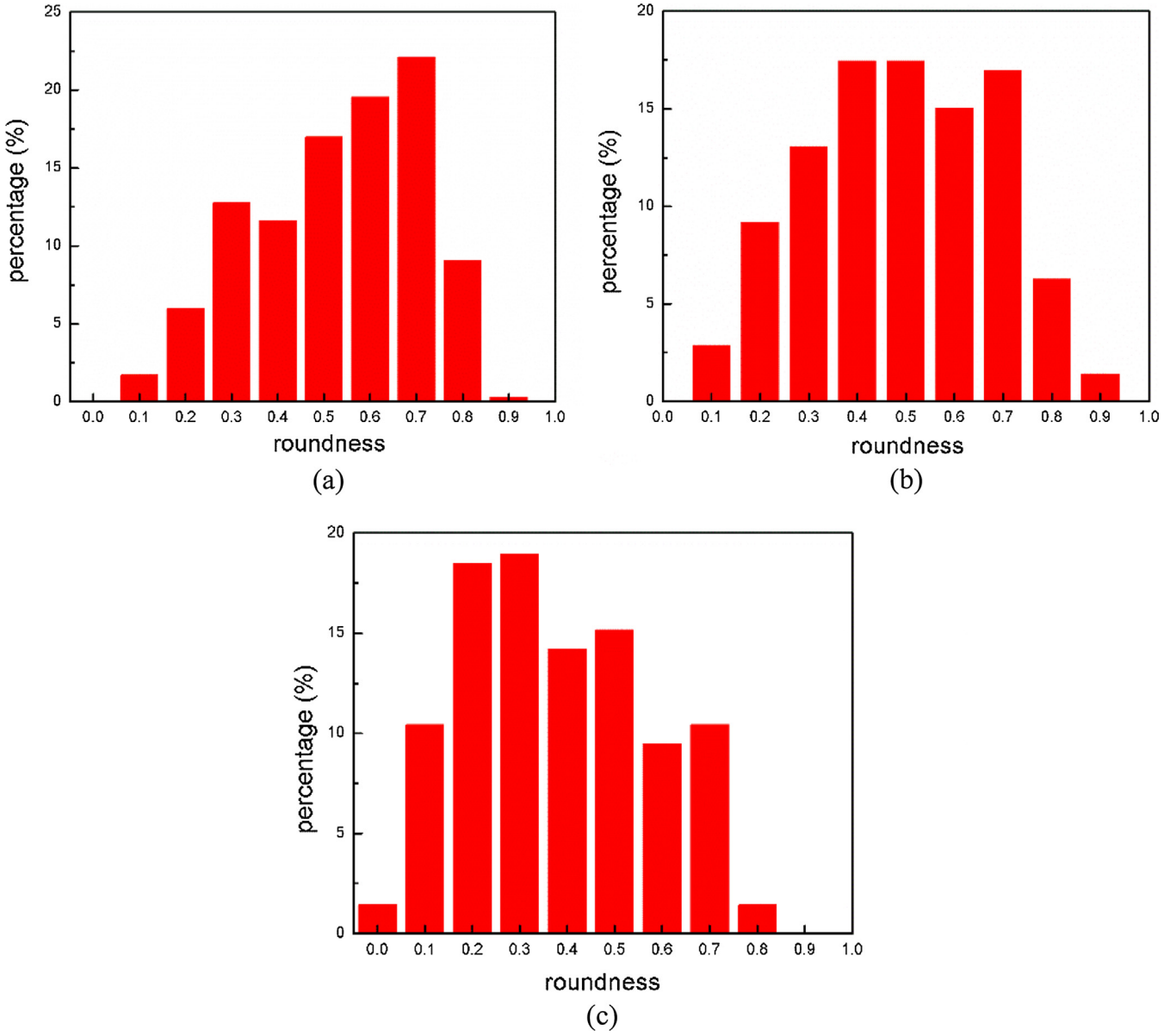

Fig. 7. The roundness distribution of the refined Si in the eutectic phase of samples processed under three different conditions (a) without UST (b) with UST applied over a range of temperature from 650 °C to 620 °C (c) with UST applied over a range of temperature from 614 °C to 600 °C during solidification.

cavitation processing from 650 °C to 620 °C. This may suggest that in Fig. 4(c), the mechanism for grain refinement is likely a combination of the increase in the nucleation potential and the promotion of the dendrite fragmentation.

3.2. The microstructure of the bottom disks

Fig. 5 shows the obtained microstructures of the bottom disks under three different experimental conditions: (1) without the use of ultrasonic cavitation processing, (2) with ultrasonic cavitation processing from 650 °C to 620 °C (which is 6 °C above the liquidus temperature), and (3) with ultrasonic cavitation processing from 614 °C to 600 °C during solidification. Fig. 5(a) was similar with Fig. 4(a), the microstructure was dendritic in shape with very large grain size. Fig. 5(b) and (c) indicated a significant refinement of the microstructure when compared with Fig. 5(a), and the grain morphology was changed from dendritic to globular. Fig. 5(b) shows similar microstructures to those shown in Fig. 4(b). However, by carefully comparing the microstructures from Fig. 5(c) with Fig. 4(c), which were taken from the bottom and the top sections of the sample processed via ultrasonic cavitation over the range of temperatures from 614 °C to 600 °C during solidification, it can be concluded that the degree of refinement of the bottom disk was not as good as that of the top disk. The reason can be explained as follows: when applying UST from 650 °C to 620 °C, all cast samples were in the liquid phase, since ultrasonic cavitation intensity was strong enough to influence the bottom section. Thus, the increase in nucleation potential would happen in the whole ingot, which would lead to the similar microstructures shown in Figs. 4(b) and 5(b). However, when applying UST from 614 °C to 600 °C during solidification, the molten melt started to solidify, and by increasing the solid phase the effect of ultrasonic cavitation and stirring is decreased, and consequently it will diminish the refinement of the microstructure.

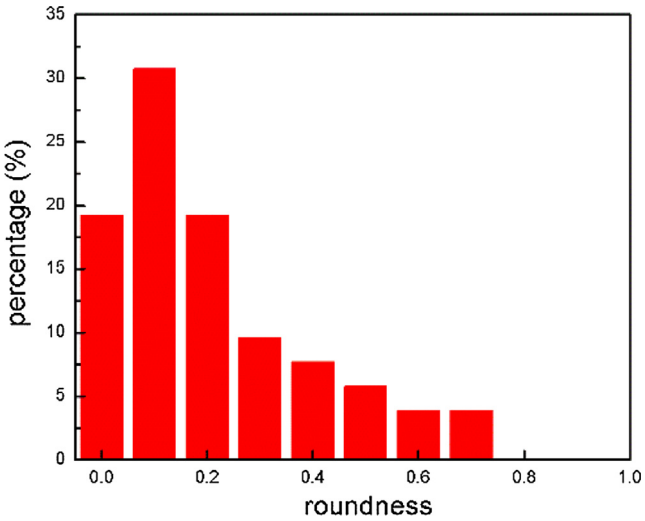

Fig. 8. The roundness distribution of the coarse Si in the eutectic phase in a processed sample without UST.

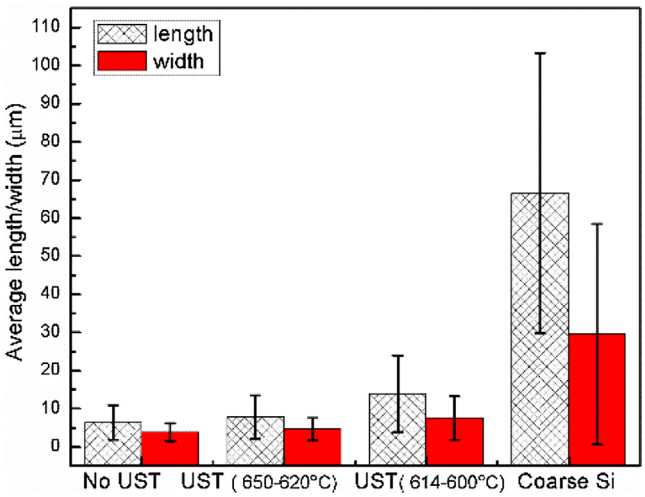

Fig. 9. Overall analysis results of the average length and width values of the Si phase in the eutectic phase.

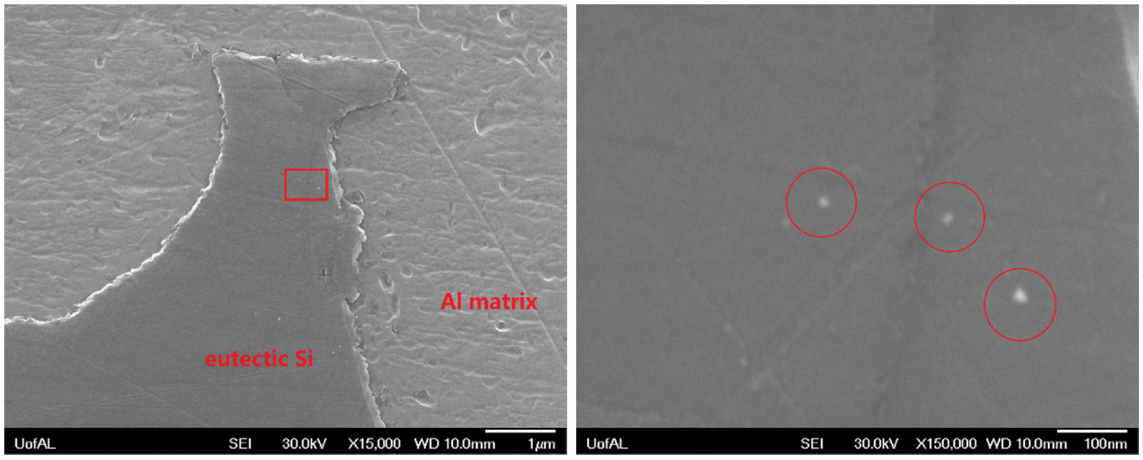

Fig. 10. SEM results of the bottom disk of the sample processed via UST over a range of temperatures from 614 °C to 600 °C during solidification (a) at 15,000× (b) at 150,000× (c) at 150,000×.

3.3. The microstructure of the eutectic phase

Fig. 6 illustrates the eutectic silicon morphology of the top disk from the cast ingots processed under three different melt treatment conditions: (1) without the use of ultrasonic cavitation processing, (2) with ultrasonic cavitation processing from 650 °C to 620 °C, and (3) with ultrasonic cavitation processing from 614 °C to 600 °C during solidification.

Fig. 6(a) indicated that A356-based Al_2O_3 nanocomposite without UST have a refined eutectic Si morphology. Fig. 6(b) and (c) shows the microstructures of the nanocomposites processed with UST from 650-620 °C and from 614 to 400 °C during solidification, respectively. The refined eutectic Si can be observed in Fig. 6 (b) and (c). However, the eutectic Si phase is coarse in all casting ingots. It should also be noted that a coarse Si morphology was still found in all processed samples. Fig. 6(d) shows the coarsest Si morphology (lamellar morphology, longer than 100 μm) that was taken from the nanocomposite sample processed without UST.

Fig. 7 presents the analysis results of the eutectic silicon morphology of alloys processed under different UST melt treatment conditions. About two hundred measurements were used for each sample to obtain the data in Fig. 7. Roundness is defined in Fig. 7 as: $4\pi A/P^2$, where A is the area of the grain, and P is the perimeter of the grain. The maximum value of roundness is 1, when the grain is a sphere. The eutectic phase in the processed A356 alloy consists of Si and Al phases growing together as a lamellar morphology. Also, in this case, the higher the roundness values of the eutectic Si phase, the higher the degree of refinement. Fig. 7(a), (b) and (c) shows that the Si roundness distribution in the processed samples with a refined eutectic morphology. Fig. 8 illustrates the roundness distribution of Si in the processed samples with a coarse eutectic morphology.

Fig. 9 presents the overall analysis results of the average length and width values of the Si in the eutectic phase. The average length of the refined Si in the eutectic phase of the samples processed without UST, with UST over a range of temperature from 650 °C to 620 °C, and with UST over a range of temperatures from 614 °C to 600 °C during solidification are 6 ± 4 μm, 8 ± 6 μm, 14 ± 10 μm, respectively. The average width of the refined Si phase in the eutectic are 4 ± 2 μm, 5 ± 3 μm, 8 ± 6 μm, respectively. The average length and width of the coarse eutectic Si are 67 ± 37 μm and 30 ± 29 μm, respectively.

As shown in Figs. 6–9, a refined Si was observed in the nanocomposite casting processed without UST, which indicates that the ultrasonic cavitation processing might not have a dominant effect on the eutectic Si modification, and the added Al_2O_3 nanoparticles might play a key role in the eutectic Si refinement. The reason could be that the Si atoms would aggregate around the Al_2O_3 nanoparticles in the melt, forming some precursors during solidification. The agglomerations and attachment of these precursors and the individual Si atoms will cause the nucleation and growth of the Si phase. However, the Si refinement is not fully complete, and because of this reason some of the formed eutectic in the cast ingots is still coarse (*i.e.*, lamellar morphology, longer than about 50 μm).

3.4. The distribution of Al_2O_3 nanoparticles

Fig. 10 presents the SEM microstructures at very high magnification of the bottom disk of the as-cast nanocomposite that was processed by applying ultrasonic cavitation over a range of temperatures from 614 °C to 600 °C during solidification. Fig. 10(a) displays the eutectic Si phase and the Al matrix under SEM observation; a rectangular section from Fig. 10(a) has been zoomed in and shown in Fig. 10(b). Fig. 10(c) shows the microstructure of the A356 matrix. The bright nanoparticles highlighted by red circles in Fig. 10(b) and (c) have spherical shape and average size of about 20 nm, which are similar in size with the nanoparticles added during the processing stage of these ingots. The SEM results indicated that the Al_2O_3 nanoparticles were dispersed reasonably well into the matrix, and no nanoparticle clusters have been found. The nanoparticles were found in both the primary matrix phase and the eutectic Si phase, which indicates that the Al_2O_3 nanoparticles were engulfed/entrapped into the solid phase and not pushed by the solid–liquid interface during solidification.

4. Conclusions

The following main conclusions were drawn from the present study:

(i) A microstructure refinement and a morphological transition from dendritic grain to globular grain structures were obtained when the ultrasonic cavitation was applied to an A356 alloy reinforced with Al_2O_3 nanoparticles during solidification.

(ii) Ultrasonic cavitation processing during solidification plays an important role to refine the microstructure by increasing the heterogeneous nucleation in the melt and by enhancing the dendrite fragmentation. A356 with Al_2O_3 nanoparticles can have globular/non-dendritic grain morphologies when ultrasonic cavitation is applied above the liquidus temperature, since Al_2O_3 nanoparticles could become active nucleation sites that would enhance the nucleation potential and consequently refine the microstructure. Ultrasonic cavitation intensity decreases along the height from the ultrasonic probe, which could diminish the dendritic fragmentation process and therefore could weaken the ultrasonic cavitation refinement process of the microstructure.

(iii) The results obtained in this study show that the areas with well modified eutectic Si phase can be observed regardless of the type of solidification conditions, which indicates that the added Al_2O_3 nanoparticles and not the application of UST during solidification would be the predominant mechanism for eutectic Si modification. However, the mechanisms of partial modification require more study.

(iv) SEM results indicated that the added Al_2O_3 nanoparticles were dispersed reasonably well into both the primary and the eutectic phases, and the Al_2O_3 nanoparticles were engulfed/ entrapped into the solid phase during the solidification process.

Acknowledgements

Yang Xuan would like to acknowledge the financial support by the China Scholarship Council (CSC).

References

[1] X.D. Liu, S.A. Jia, L. Nastac, Ultrasonic cavitation-assisted molten metal processing of cast A356-nanocomposites, Int. J. Metalcasting, AFS 8 (3) (2014) 51–58.

[2] A.B. Elshalakany, T.A. Osman, A. Khattab, B. Azzam, M. Zaki, Microstructure and mechanical properties of MWCNTs reinforced A356 aluminum alloys cast nanocomposites fabricated by using a combination of rheocasting and squeeze casting techniques, J. Nanomater. (2014).

[3] B. Su, H.G. Yan, G. Chen, J.L. Shi, J.H. Chen, P.L. Zeng, Study on the preparation of the SiCp/Al-20Si-3Cu functionally graded material using spray deposition, Mater. Sci. Eng. A-Struct. 527 (24–25) (2010) 6660–6665.

[4] D. Bozic, B. Dimcic, O. Dimcic, J. Stasic, V. Rajkovic, Influence of SiC particles distribution on mechanical properties and fracture of DRA alloys, Mater. Des. 31 (1) (2010) 134–141.

[5] M.P. De Cicco, X.C. Li, L.S. Turng, Semi-solid casting (SSC) of zinc alloy nanocomposites, J. Mater. Process Tech. 209 (18–19) (2009) 5881–5885.
[6] S.M.S. Reihani, Processing of squeeze cast A16061–30vol% SiC composites and their characterization, Mater. Des. 27 (3) (2006) 216–222.
[7] C.S. Goh, J. Wei, L.C. Lee, A. Gupta, Simultaneous enhancement in strength and ductility by reinforcing magnesium with carbon nanotubes, Mater. Sci. Eng. A-Struct. 423 (1–2) (2006) 153–156.
[8] D.Y. Ying, D.L. Zhang, Processing of Cu-Al_2O_3 metal matrix nanocomposite materials by using high energy ball milling, Mater. Sci. Eng. A-Struct. 286 (1) (2000) 152–156.
[9] S. Jia, D. Zhang, Y. Xuan, L. Nastac, An experimental and modeling investigation of aluminum-based alloys and nanocomposites processed by ultrasonic cavitation processing, Appl. Acoust. 103 (2016) 226–231.
[10] Y. Xuan, S. Jia, L. Nastac, Processing and microstructure characteristics of as-cast A356 alloys manufactured via ultrasonic cavitation during solidification, High Temp. Mater. Process 36 (4) (2017) 381–387.
[11] K. Borodianskiy, A. Kossenko, M. Zinigrad, Improvement of the mechanical properties of Al-Si alloys by TiC nanoparticles, Metall. Mater. Trans. A. 44a (11) (2013) 4948–4953.
[12] M.K. Akbari, O. Mirzaee, H.R. Baharvandi, Fabrication and study on mechanical properties and fracture behavior of nanometric Al_2O_3 particle-reinforced A356 composites focusing on the parameters of vortex method, Mater. Des. 46 (2013) 199–205.
[13] M.K. Akbari, H.R. Baharvandi, O. Mirzaee, Fabrication of nano-sized Al_2O_3 reinforced casting aluminum composite focusing on preparation process of reinforcement powders and evaluation of its properties, Compos. Part B-Eng. 55 (2013) 426–432.
[14] Y. Yang, J. Lan, X.C. Li, Study on bulk aluminum matrix nano-composite fabricated by ultrasonic dispersion of nano-sized SiC particles in molten aluminum alloy, Mater. Sci. Eng. A-Struct. 380 (1–2) (2004) 378–383.
[15] Xiaoda Liu, Fundamental Studies on Ultrasonic Cavitation-assisted Molten Metal Processing of a356-Nanocomposites, The University of Alabama, 2013.
[16] S.A. Jia, Y. Xuan, L. Nastac, P.G. Allison, T.W. Rushing, Microstructure, mechanical properties and fracture behavior of 6061 aluminium alloy-based nanocomposite castings fabricated by ultrasonic processing, Int. J. Cast. Metal. Res. 29 (5) (2016) 286–289.
[17] J.C. Yan, Z.W. Xu, L. Shi, X. Ma, S.Q. Yang, Ultrasonic assisted fabrication of particle reinforced bonds joining aluminum metal matrix composites, Mater. Des. 32 (1) (2011) 343–347.
[18] J. Lan, Y. Yang, X.C. Li, Microstructure and microhardness of SiC nanoparticles reinforced magnesium composites fabricated by ultrasonic method, Mat. Sci. Eng. A-Struct. 386 (1–2) (2004) 284–290.
[19] X. Jian, H. Xu, T.T. Meek, Q. Han, Effect of power ultrasound on solidification of aluminum A356 alloy, Mater. Lett. 59 (2–3) (2005) 190–193.
[20] X.B. Liu, Y. Osawa, S. Takamori, T. Mukai, Grain refinement of AZ91 alloy by introducing ultrasonic vibration during solidification, Mater. Lett. 62 (17–18) (2008) 2872–2875.
[21] G. Wang, M.S. Dargusch, M. Qian, D.G. Eskin, D.H. StJohn, The role of ultrasonic treatment in refining the as-cast grain structure during the solidification of an Al-2Cu alloy, J. Cryst. Growth 408 (2014) 119–124.
[22] Gui Wang, Matthew S. Dargusch, David H. StHohn, Effect of ultrasonic treatment on the as-cast grain structure during the solidification of an Al-2Cu alloy, in: T. Furuhara, M. Nishida, S. Miura (Eds.), The Ninth Pacific Rim International Conference on Advanced Materials and Processing (PRICM9), Aug. 1–5, The Japan Institute of Metals and Materials, Kyoto City, 2016.
[23] A. Ramirez, M. Qian, B. Davis, T. Wilks, High-intensity ultrasonic grain refinement of magnesium alloys: role of solute, Int. J. Cast. Metal. Res. 22 (1–4) (2009) 260–263.
[24] M. Qian, A. Ramirez, Ultrasonic grain refinement of magnesium and its alloys, in: F. Czerwinski, (Ed.), Magnesium Alloys – Design, Processing and Properties, InTech, 2011, pp. 163–186.
[25] H.K. Feng, S.R. Yu, Y.L. Li, L.Y. Gong, Effect of ultrasonic treatment on microstructures of hypereutectic Al-Si alloy, J. Mater. Process. Tech. 208 (1–3) (2008) 330–335.
[26] J.I. Youn, Y.J. Kim, Nucleation enhancement of Al alloys by high intensity ultrasound, Jpn. J. Appl. Phys. 48 (7) (2009).
[27] J.G. Jung, S.H. Lee, J.M. Lee, Y.H. Cho, S.H. Kim, W.H. Yoon, Improved mechanical properties of near-eutectic Al-Si piston alloy through ultrasonic melt treatment, Mater. Sci. Eng. A-Struct. 669 (2016) 187–195.
[28] Jeong I.L. Youn, Young Ki Lee, Young Jig Kim, J.W. Park, Effect of sonotrode material on grain refining of Mg–3Al and Mg–9Al alloys by ultrasonic melt treatment, Jpn. J. Appl. Phys. 55 (07KE10) (2016), 07KE10-1–07KE10-6.
[29] S.L. Zhang, Y.T. Zhao, X.N. Cheng, G. Chen, Q.X. Dai, High-energy ultrasonic field effects on the microstructure and mechanical behaviors of A356 alloy, J. Alloy. Compd. 470 (1–2) (2009) 168–172.
[30] D.M. Herlach, K. Eckler, A. Karma, M. Schwarz, Grain refinement through fragmentation of dendrites in undercooled melts, Mater. Sci. Eng., A. 304–306 (2001) 20–25.